Article

MXene/Ag$_2$CrO$_4$ Nanocomposite as Supercapacitors Electrode

Tahira Yaqoob [1], Malika Rani [1,*], Arshad Mahmood [2], Rubia Shafique [1], Safia Khan [3], Naveed Kausar Janjua [3], Aqeel Ahmad Shah [4], Awais Ahmad [5] and Abdullah A. Al-Kahtani [6]

[1] Department of Physics, The Women University Multan, Multan 66000, Pakistan; tahiraroy123@gmail.com (T.Y.); rubiashafique@yahoo.com (R.S.)

[2] National Institute of Lasers and Optronics (NILOP), College PIEAS, NILORE, Islamabad 45650, Pakistan; drarshadjanjua@gmail.com

[3] Department of Chemistry, Quaid-I-Azam University, Islamabad 45320, Pakistan; safiakhan715@gmail.com (S.K.); nkausarjanjua@yahoo.com (N.K.J.)

[4] Department of Metallurgical Engineering, NED University of Engineering and Technology, Karachi 75270, Pakistan; gr8muet@gmail.com

[5] Departamento de Quimica Organica, Universidad de Cordoba, Edificio Marie Curie (C-3), Ctra Nnal IV-A, Km 396, E14014 Cordoba, Spain; awaisahmad@gcuf.edu.pk

[6] Chemistry Department, College of Science, King Saud University, Riyadh 11451, Saudi Arabia; akahtani@ksu.edu.sa

* Correspondence: dr.malikarani@yahoo.com

Abstract: MXene/Ag$_2$CrO$_4$ nanocomposite was synthesized effectively by means of superficial low-cost co-precipitation technique in order to inspect its capacitive storage potential for supercapacitors. MXene was etched from MAX powder and Ag$_2$CrO$_4$ spinel was synthesized by an easy sol-gel scheme. X-Ray diffraction (XRD) revealed an addition in inter-planar spacing from 4.7 Å to 6.2 Å while Ag$_2$CrO$_4$ nanoparticles diffused in form of clusters over MXene layers that had been explored by scanning electron microscopy (SEM). Energy dispersive X-Ray (EDX) demonstrated the elemental analysis. Raman spectroscopy opens the gap between bonding structure of as-synthesized nanocomposite. From photoluminence (PL) spectra the energy band gap value 3.86 eV was estimated. Electrode properties were characterized by applying electrochemical observations such as cyclic voltammetry along with electrochemical impedance spectroscopy (EIS) for understanding redox mechanism and electron transfer rate constant K$_{app}$. Additionally, this novel work will be an assessment to analyze the capacitive behavior of electrode in different electrolytes such as in acidic of 0.1 M H$_2$SO$_4$ has specific capacitance C$_{sp}$ = 525 F/g at 10 mVs^{-1} and much low value in basic of 1 M KOH electrolyte. This paper reflects the novel synthesis and applications of MXene/Ag$_2$CrO$_4$ nanocomposite electrode fabrication in energy storage devices such as supercapacitors.

Keywords: MXene nanocomposite; spinel chromite; energy storage; supercapacitors electrodes

1. Introduction

The stipulate for well-groomed energy storage strategies is on the hit list in the current state of affairs. To overcome this worldwide issue, supercapacitors were used to pile up energy in electronic applications to store charge, depending upon electrochemical reactions enclosed by them [1]. Narrative layered two-dimensional (2D) material i.e., MXene (Ti$_3$C$_2$T$_x$) comprehensively deliberated to construct electrodes for supercapacitors owing to their high metallic conduction rate and reactive hydrophilic surface. In spite of all the assorted dilemmas including re-crushing and oxidizing of titanium which obstruct Ti$_3$C$_2$T$_x$ to achieve the significant capacitance, cheap carbon electrode material for instance Ti$_3$C$_2$T$_x$, a type of MXene, participated in great technological research for development of supercapacitors electrodes by defeating these issues [2–4]. In composite form, Ti$_3$C$_2$T$_x$ deals with the above-mentioned problems due to its excellent specific capacity with lower resistance, significant surface area and the redox active nature of surface

functional groups. Supercapacitors (SCs) had been discussed as a promising energy storage tool due to the fast charge/discharge process, high power density in many new technologies and the use of the redox (pseudo-capacitive) mechanism on surface which could be employed for storing more energy than batteries [5–7]. The electrochemical capacitors (ECs) mentioned as supercapacitors are taken as the key technology for the promotion of the immense progress in 2D transition metal carbides/nitrides, known as "MXene". Hence, MXene ($Ti_3C_2T_x$) showed potential as electrode resource of supercapacitors due to their key factors of intercalation, pseudocapacitance mechanism, metallic-like conductivity, power and energy storing aptitude [8,9]. The MXene in bare form obsessed low specific capacitance about 246 (F/g) in supercapacitors, but it improved its capacitive nature, significant specific surface area, hydrophilic nature, porous structure, negatively charged surfaces by recombination with other materials in nanocomposite form [10–13]. In energy storage applications i.e., in supercapacitors the transition metal oxides (TMOs) exhibited mixed spinal structure because of remarkable electrochemical properties were taken into consideration [14,15]. Hence metal oxide systems including metal chromite spinels, for instance $MgCr_2O_4$ [16] and $CaCr_2O_4$ [17], these exceptional spinels are verified to be high-performance electrode materials for electrochemical supercapacitors which may be taken either in single or in composite form with carbon-based materials for better results [18]. Among various silver-based compounds, (Ag_2CrO_4) nanoparticles in which crystallization occurred in orthorhombic form [19], Ag_2CrO_4 in composite form such as (Ag_2CrO_4/GO) composites [20], TiO_2/Ag_2CrO_4 nanocomposites [21], Ag_2CrO_4/g-C_3N_4, RuO_2-MXene along with silver, Co_3O_4/MXene, MXene/Ag, TiO_2/Ti_3C_2, lanthanum and manganese co-doped bismuth ferrite/Ti_3C_2, MXene ($Ti_3C_2T_x$)/Ag NWs (silver nanowires) had been synthesized in the past for various energy storage purposes [22–30]. The most recent work done on copper-chromite/graphene-oxide nanocomposite for electrode fabrication explored new energy tools had been accepted in my own collaboration [31]. However, there was no earlier work done in this field until now and thus this paper can be claimed as a novel work. The affordable wet chemical co-precipitation sonicated-assisted mechanical method of mixing was practiced during synthesis process of MXene/Ag_2CrO_4 nanocomposite which made it fit candidate for supercapacitive applications. Ag_2CrO_4 nanoparticles adding up with MXene sheets enhanced the capacitive properties of MXene by generating a course to electron transfer that led to unique surface contact within MXene sheets. We put forward the challenges and perspectives for the future progress of the MXene/Ag_2CrO_4 nanocomposite.

2. Materials and Methods

2.1. Chemical and Reagents

Silver nitrate pentahydrate (99.0%), chromium nitrate monohydrate (99%), 1, 2 ethanediol (99.8% pure) and powder form of tin was used. Here acetic acid (99.9%) acting as a catalytic agent, ethylene glycol (99.5%) was engrossed in it both for solution and reduction. Additionally, hydrofluoric acid known as HF (39%) was applied as etching agent in MAX (Ti_3AlC_2) powder. Deionized water (DI) was used as a solvent. The chemicals collected from sigma Aldrich company were used.

2.2. Ag_2CrO_4 Nanoparticles Synthesis

In order to synthesize Ag_2CrO_4 nanoparticles, the wet chemical sol-gel method was applied. In this approach, 4 g of silver nitrate and 3 g of chromium nitrate solution was prepared in 50 mL of DI water accomplished by adding up of citric acid powder in 2:1 ratio. The aqueous solution undergone continuous stirring at 70 °C until the required homogeneous solution obtained. After viscous gel development, stirring had been stopped. In order to achieve main product, solution was positioned at oven adjusted at 700 °C for three hours and then further calcination at 600 °C in the furnace was performed. At the end, powder form of the sample grounded in agate motor to get homogeneous fine powder.

The chemical formula of Ag_2CrO_4 was explained by chemical Equations (1) and (2) given below [32].

$$Ag = Ag^+ + e^- \tag{1}$$

$$2Ag^+ + CrO_4{}^{-2} = Ag_2CrO_4 \tag{2}$$

The obtained powder of Ag_2CrO_4 nanoparticles was used to synthesize nanocomposite of MXene/Ag_2CrO_4.

2.3. Synthesis of MXene (Ti$_3$C$_2$T$_x$)

MXene was synthesized using the conventional method. First, 10 g of formerly prepared MAX powder were taken in a teflon bottle with 200 mL (39%) intense HF to synthesize $Ti_3C_2T_x$ (MXene). Hydrofluoric acid (HF) and MAX powder was homogeneously blended by constant stirring for 36 h, at room temperature. Later, the hot plate was removed, and the solution was placed to cool down for 12 h. Moreover, the mixture was again stirred for 12 h. At the end, the resultant solution was rinsed several times by using deionized (DI) water followed by vacuum filtration. By drying the solution at 60 °C for 12 h, the etched MXene obtained is used for assembling of nanocomposite [33].

2.4. Synthesis of MXene/Ag$_2$CrO$_4$ Nanocomposite

The easily available wet chemical method, namely the co-precipitation method, was used to synthesize nanocomposite of MXene/Ag_2CrO_4 in which the solution of MXene prepared in 200 mL DI water by taking 200 mg of $Ti_3C_2T_x$ (MXene) under sonication for 10 min. At the same time already prepared Ag_2CrO_4 nanoparticles were assorted in 100 mL acetic acid and 100 mL ethylene glycol in a stoichiometric proportion of 1:1 with 0.01 M (morality). Sonication of MXene solution was performed at 3500 rpm for 120 min at 60 °C to obtain homogeneous sample. Then, both solutions were thoroughly mixed by continuous stirring at 80 °C for 1 hr. After that the settled solution was washed many times with DI water unless neutral solution was obtained. An oven was used at 70 °C for 24 h until it is completely dried. Obtained nano-powder became homogenous using an agate motor.

3. Results and Discussion

3.1. X-ray Diffraction (XRD) Analysis

The structure of the resultant sample was analyzed by X-Ray diffraction (XRD) technique with monochromatic wavelength λ (1.5 Å) in which corresponding (hkl) values were assigned approximately to all peaks. In Figure 1, the XRD pattern of bare Ag_2CrO_4 nanoparticles representing an orthorhombic structure with the JCPDS no. 026-0952 in which Bragg diffraction peaks appeared at 2θ = 24.45°, 33.65°, 36.34°, 37.92°, 43.82°, 47.97°, 50.36°, 54.95°, 57.91°, 63.42°, 67.18° confirming successful synthesis of Ag_2CrO_4 nanoparticles [34]. The prominently solid and high-pitched peaks proved pure and well-crystalline Ag_2CrO_4 collected by the stated process [35]. The characteristic peaks of MAX at 9.5° and 19.2° angles with (002) and (004) planes transferred towards left due to etched aluminum (Al) peaks resulting an increase in the spacing between sheets of resulting etched MAX powder so-called MXene ($Ti_3C_2T_x$) [36]. In MXene/Ag_2CrO_4 nanocomposite all the peaks shifted towards lower angles with low intensity, certified an increase in inter-planar spacing from 4.7 Å to 6.2 Å of MXene/Ag_2CrO_4 nanocomposite which step up the conductivity [37].
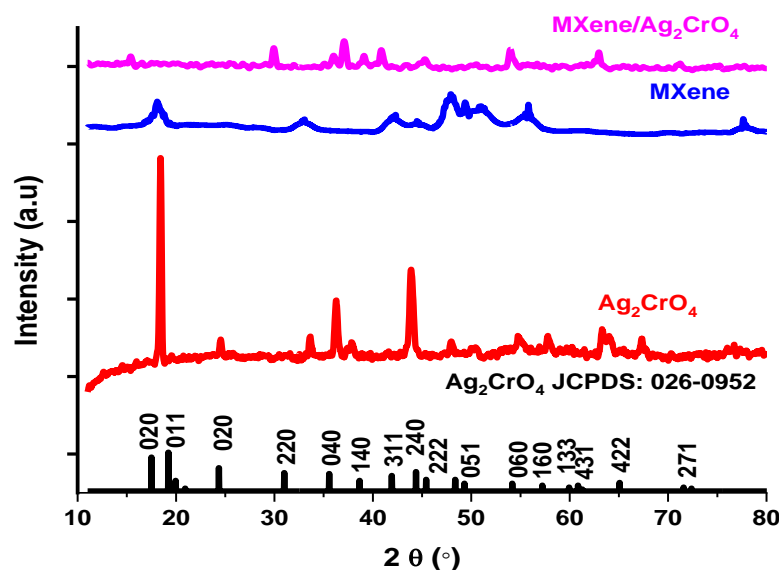
Figure 1. XRD patterns of Ag_2CrO_4, MXene and MXene/Ag_2CrO_4 nanocomposite.

From XRD data [38] the average crystallite size of MXene/Ag_2CrO_4 nanocomposite was calculated by Debye-Scherrer Equation (3) given below.

$$D = K\lambda/(\beta\, Cos\theta) \tag{3}$$

In general, crystalline size D in nm, X-ray wavelength λ is 0.15 nm, θ is the Bragg's angle in radian, β full width half maximum of diffracted beams. The average crystallite size of MXene/Ag_2CrO_4 nanocomposite is 14 nm analogous to other MXene composite [39,40]. The presence of characteristic peaks of Ag_2CrO_4 and MXene in the nanocomposite sample is an indication of the successful development of MXene/Ag_2CrO_4 nanocomposite.

3.2. The Scanned Electronic Microscopic Analysis

The scanned electron microscopic (SEM) analysis of the synthesized sample explained the surface morphology of MXene/Ag_2CrO_4 nanocomposite. The purpose was to see how MXene and Ag_2CrO_4 nanoparticles coordinated with each other, including the even and continuous layered form of MXene with sharp edges gained after selective etching of aluminum (Al) layer by HF etching method as shown in Figure 2a. The SEM images of the $Ti_3C_2T_x$/Ag_2CrO_4 nanocomposite sample are shown in Figure 2b in which nanoparticles of Ag_2CrO_4 adorned the surface of $Ti_3C_2T_x$ in random pattern forming coagulated structure and explored huge clusters of the nanoparticles. Hence, only some grains scattered on layers of MXene. The number of nanoparticles nucleated on the surface of MXene engraved pores caused more storage capacity [41–44]. The average diameter of Ag_2CrO_4 nanoparticles is 75 nm reported in [32], here 3.67 nm is the grain size of MXene/Ag_2CrO_4 nanocomposite calculated by using image J. software. Here, clearly, it can be seen Ag_2CrO_4 nanoparticles in the MXene/Ag_2CrO_4 nanocomposite were reduced suggestively and closely occupied the MXene sheets. Furthermore, grain size distribution histogram shown in Figure 3 summarizing discrete or continuous data on an interval scale, respectively.
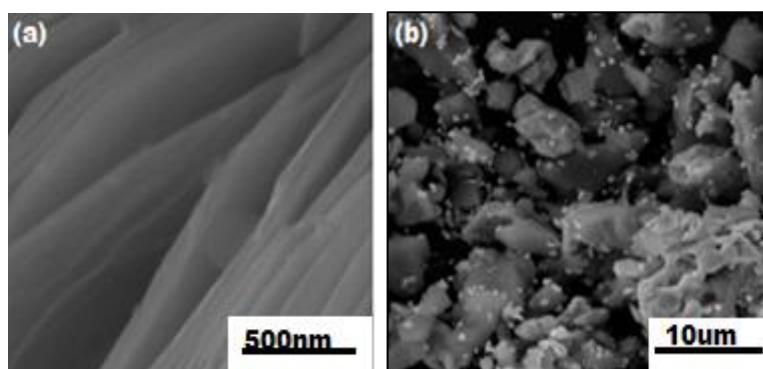
Figure 2. Images obtained from SEM of (**a**) MXene ($Ti_3C_2T_x$), (**b**) MXene/Ag_2CrO_4 nanocomposite.
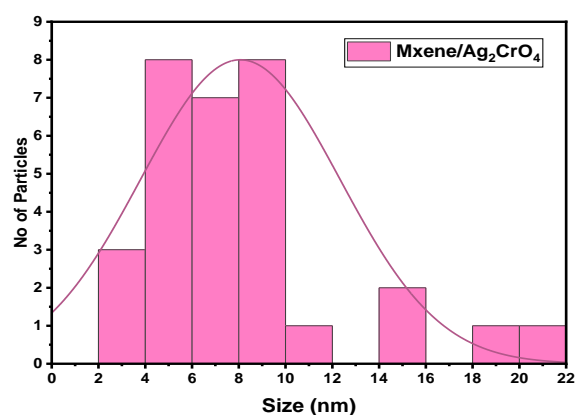

Figure 3. Particle size distribution histogram determined by SEM images.

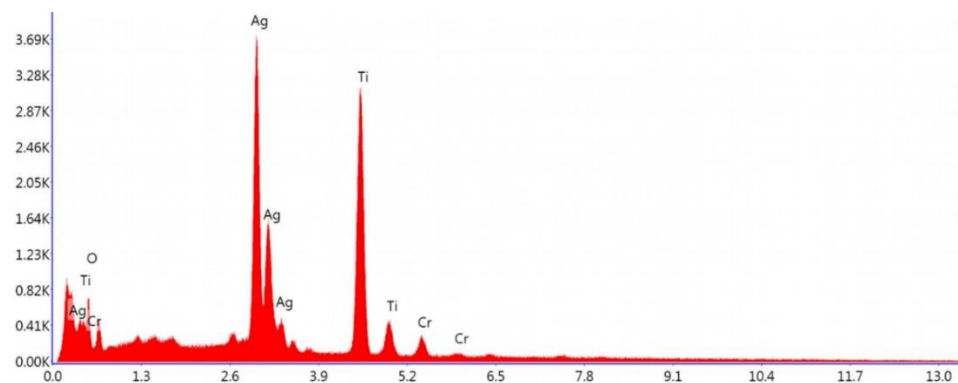*3.3. Energy Dispersive X-ray Spectroscopy (EDX)*

The spectroscopy of energy dispersion analysis of Ag_2CrO_4 nanoparticles and MXene/ Ag_2CrO_4 powder are exhibited in Figure 4a,b, respectively, where not only the Ag, Cr and Ti signals seemed but also the O signal appeared due to oxidation of MXene concerned with some functional groups. This provided the proof of perfect synthesis of current nanocomposite [45]. The elements presented in spectra as per EDX analysis according to weight percentage is confirmation of the ideal synthesis of the required MXene/Ag_2CrO_4 nanocomposite as shown in Table 1.

Table 1. Estimated elemental composition of MXene/Ag_2CrO_4 nanocomposite.

Elements	Shell	Weight (%)
Oxygen	K	14.10
Silver	K	43.41
Titanium	K	39.04
Chromium	K	3.04
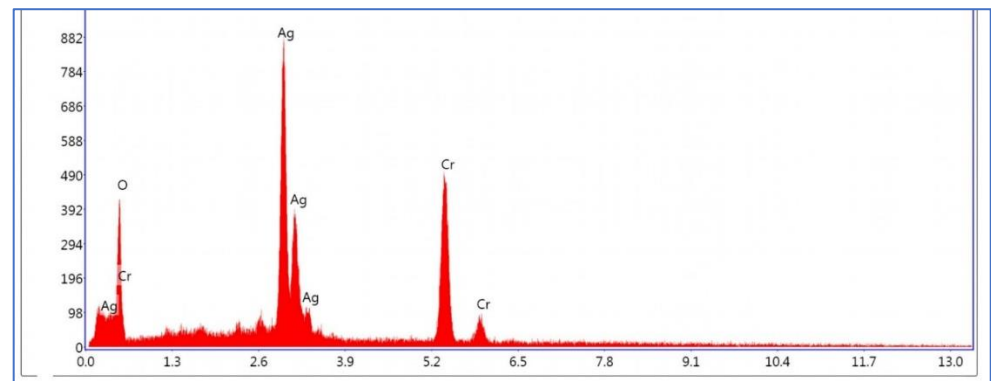
(a)

(b)

Figure 4. Energy dispersive spectra of (**a**) Ag_2CrO_4 nanoparticles (**b**) MXene/Ag_2CrO_4 nanocomposite.

3.4. Raman Spectroscopy

Here, Raman spectroscopy has been employed to illustrate extremely responsive composition of the material structure having incredibility and a more mechanically important spectroscopic technique to probe the dynamic vibrational phonons of $Ti_3C_2T_x$/Ag_2CrO_4 nanocomposite [46]. The Raman spectra of MXene ($Ti_3C_2T_x$) was determined at 155 cm^{-1} showing a vibrational band of anatase phase of TiO_2 [47]. Phonons (lattice vibrations) at the interface of MXene and traces of transition metal oxides were handled by Raman spectroscopy. Two main causes of lattice viberations in MXene based materials one, surface functional groups involved stimulating pseudocapacitance and the other, exchanging of ion gave rise to storing charge leading to a high capacitance of MXene/Ag_2CrO_4 nanocomposite in acidic solution [48,49].

Raman spectroscopy of MXene/Ag_2CrO_4 nanocomposite noted at wavelength 532 nm and power 150 mW showing a characteristic peak at definite position 0.86 cm^{-1} with a remarkable intensity confirmed the occurrence of the prepared nanocomposite mostly due to the existence of functional groups involed [50] as shown in Figure 5.
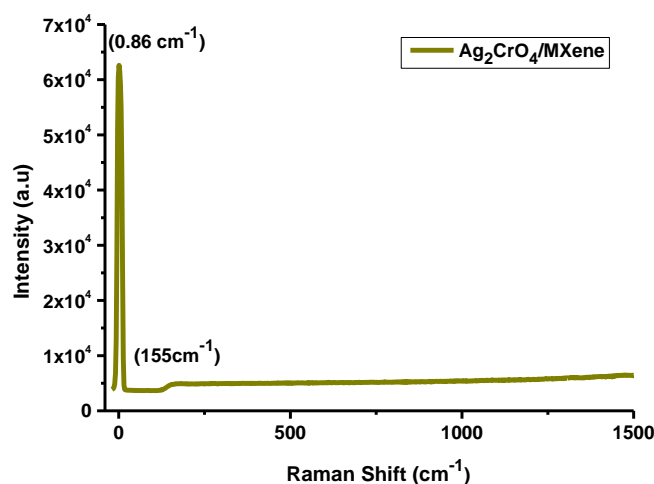
Figure 5. Raman spectra of MXene/Ag_2CrO_4 nanocomposite.

3.5. Photoluminescence (PL) Spectroscopy

The optical spectra of MXene/Ag_2CrO_4 nanocomposites were explained by using 325 nm wavelength of He-Cd laser at room temperature with 40 MW power. At 300 nm wavelength, the optical band gap 3.86 eV calculated in the visible region is indication of the allocation of nanoparticles clearly seen in Figure 6. The photoluminescence (PL) spectra of $Ti_3C_2T_x$/Ag_2CrO_4 nanocomposite explored high intensity emission peak at 321 nm which was mainly due to electron-hole pair recombination of sp^2 hybridized carbon atoms [51,52]. Due to defects in the structure of Ag_2CrO_4 the photoluminescence emission properties were possible at room temperature [34]. The recommended speed of charges transported by light irradiation effect on the $Ti_3C_2T_x$/Ag_2CrO_4 nanocomposite in which valence band (VB) negative charges near to the ground skip to the conducting band (CB) due to complex photoluminescence scheme. When light was projected, positive and negative charges in aqueous medium coupled to produce radicals on the exterior of the $Ti_3C_2T_x$/Ag_2CrO_4 nanocomposite [53].
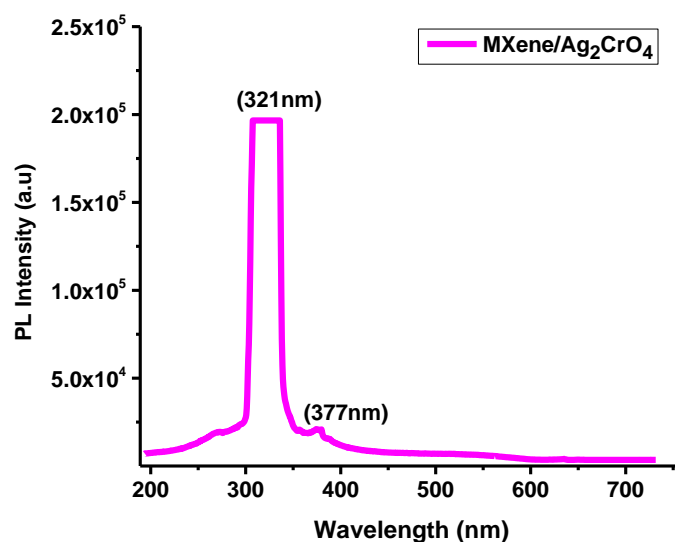

Figure 6. PL spectrum of $Ti_3C_2T_x$/Ag_2CrO_4 nanocomposite.

3.6. Electrochemical Analysis

In order to perform the electrochemical analysis at Gamry potentiostat interface 1000, a three electrode assembly was taken where platinum wire, glassy carbon electrode (GCE) and Ag/AgCl were used as counter, working and reference electrodes, respectively [54,55]. The working electrode was rinsed many times using an alumina slurry and ethanol prior

to production of synthesis material. To fabricate GCE, 0.25 g powder of electrode material was used with 2 μL of 5% nafion solution on glassy carbon electrode [56]. The functional electrode underwent drying in an oven at 50 °C for 20 min.

3.6.1. Electrochemical Impedance Spectroscopy (EIS)

The electrochemical impedance spectroscopy (EIS) was adopted to study the dependence of capacitance of supercapacitors on the applied power in which an alternating current voltage of 0.5 V and zero direct current voltage was utilized and current passes through electrode (metal or semiconductors) at working position [57]. The electron transferred properties of $Ti_3C_2T_x/Ag_2CrO_4$ were studied by using EIS. The Nyquist plots drawn for $Ti_3C_2T_x/Ag_2CrO_4$ in 0.1 M H_2SO_4 and 1 M KOH were displayed in Figure 7, also concerned EIS parameters were given in Table 2. The differences in electrochemical behavior of the as-synthesized electrocatalysts depend upon the relative feasibility of electron transfer. Low charge transfer resistance R_p due to elevated conduction, facilitated more electrons in the electrode surface and the current electrocatalysts showed a low R_p value [58] with high conductivity in acidic media, hence a higher specific capacitance C_{sp} value was achieved. The nature of the electrodes exhibited no influence on the solution resistance (Ru) and Warburg resistance (Rw) because these are features of the electrolyte and diffusion of electroactive specie that are common in all observations. However, (R_p) and phase constant element (CPE) are influenced by modification of electrodes, as they are associated with conductive properties of the active material. Here α represents surface roughness factor and its value varies from 0 to 1. Herein, currently modified electrode system has α value 0.85 and 0.89 revealing that catalysts depicted enough surface roughness. The electron-transfer rate constant K_{app} (cm s^{-1}) for planned catalysts was deliberated using the following Equation (4) [59]. Moreover, the fitted EIS model i.e., CPE with the diffusion model has been represented in the inset of Nyquist plots in Figure 7.
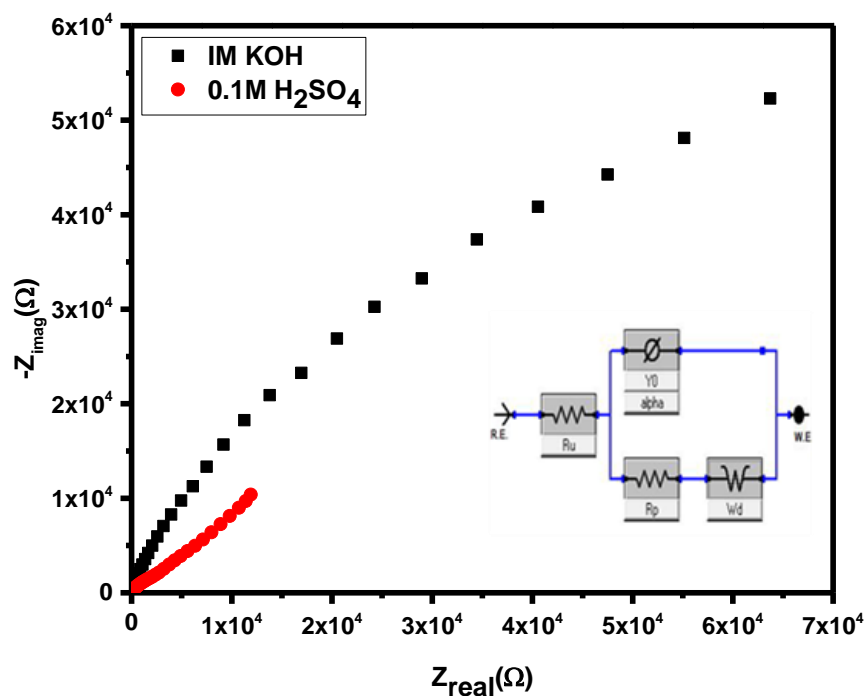
$$k_{app} = RT/F^2 \cdot R_p \cdot C \tag{4}$$

Figure 7. Nyquist plots of $Ti_3C_2 T_X/Ag_2CrO_4$ in 1 M KOH and 0.1 M H_2SO_4..

Table 2. Electrochemical parameters estimated from EIS analysis $Ti_3C_2T_x/Ag_2CrO_4$ modified electrode.

| Electrolyte	R_u (Ω)	R_p $(k\Omega)$	CPE (μF)	Alpha	R_W $(\mu\Omega)$	K_{app} $(10^{-8}\,cm\,s^{-1})$
1M KOH	17.52	52.60	7.90	0.85	19.63	0.03
0.1M H_2SO_4	7.80	$1.35e^{-6}$	0.94	0.89	92.03	3953

Here, F served as the Faraday constant, C corresponds to amount of analyte and R is the universal constant in SI units.

The poorer K_{app} in 1 M KOH aqueous electrolyte solution corresponds to relatively lower electron conductivity as compared to acidic electrolyte.

3.6.2. Electrochemical Active Surface Area (ECSA) Analysis

The electrochemically active surface area (ECSA) is an important performance indicator of a catalyst in any electrochemical reaction and for this reason cyclic voltammograms of all prepared electrocatalysts were recorded in a standard redox solution of 5 mM potassium ferrocyanide ($K_4[Fe\,(CN)_6]$) and 3M potassium chloride (KCl) at 100 mVs^{-1} for ECSA inference [60]. Peak current (i_p) increment in the CV profile correspond to a reversible one-electron transfer process using the synthesized nanocomposite as modified electrodes in $K_4[Fe\,(CN)_6]$ electrolyte. This observation of a reversible CV profile was used to point out the oxidation and reduction methods by an overall redox process as shown in Figure 8. The ECSA of electrode was calculated by applying the Randles-Sevcik Equation (5) [61].

$$i_p = 2.69 \times 10^5 \cdot n^{3/2} \cdot A \cdot D^{1/2} \cdot \upsilon^{1/2} \cdot C \tag{5}$$
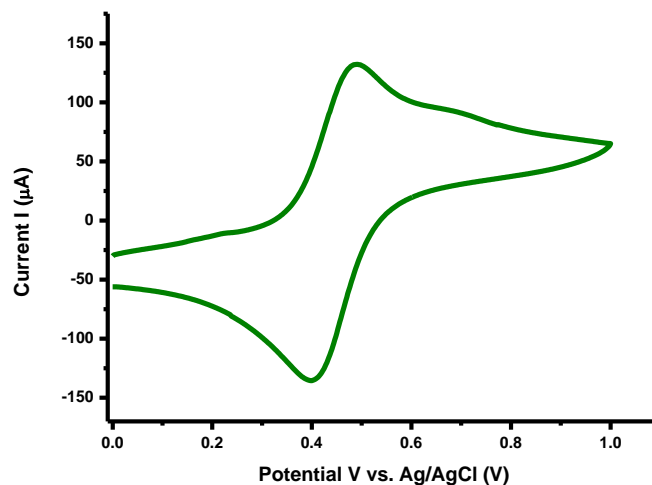
Figure 8. Cyclic voltammogram Fe^{2+}/Fe^{3+} redox couple on $Ti_3C_2T_x/Ag_2CrO_4$ modified GCE in 5 mMK$_4$[Fe (CN)$_6$]) + 3M KCl at 100 mVs^{-1}.

Here i_p is the peak current, n is the count of transferred electrons, A is the electrochemical active surface area (cm^2), D corresponds to the diffusion co-efficient, υ represents the scan rate (Vs^{-1}), C is analytic amount [62]. With a peak current value of 132 μA, the ECSA of observed electrode is 0.04 cm^2 that referred to efficient capacitive performance of the electrode material.

3.6.3. Electrochemical Investigations

The electrochemical performances of $Ti_3C_2T_x/Ag_2CrO_4$ nanocomposite were evaluated by cyclic voltammetry (CV) by varying the electrode potential between a working electrode and reference electrode in order to measure current flows between working and counter electrodes. By using the modified working electrodes in both acidic and basic

electrolytes to analyze the electrode potential in both media, the acid electrolyte has the advantage in providing protons for as synthesized nanocomposite in cyclic voltammetry [63]. The capacitive behavior of the nanocomposite was observed in forward and reverse directions relative to the anodic peaks (oxidation) and cathodic peaks (reduction) which is the verification of surface redox reactions. The specific capacitance of working electrode $Ti_3C_2T_x/Ag_2CrO_4$ nanocomposite was calculated using Equation (6).

$$C_{sp} = A/2 \ [mkV] \tag{6}$$

where C_{sp} is specific capacitance in F/g, m is used for mass of electrode i.e., 0.25 mg, k represents the scan rate and A denotes integrated area under CV curve and V corresponds to potential window -0.2 V to 0.6 V. The estimated electrochemical capacitance parameters are summarized in Table 3.

Table 3. Specific capacitance measurements from cyclic voltametric measurements.

Scan Rate (m Vs^{-1})	Specific Capacitance (F/g) in 1 M KOH	Specific Capacitance (F/g) in 0.1 M H$_2$SO$_4$
10	-	525
20	75	348
40	40	239
70	29	176
80	28	161
100	26	148

Cyclic voltammetry demonstrated capacitive performance of $Ti_3C_2T_x/Ag_2CrO_4$ electrode at different scan rate as shown in Figure 9. The highest C_{sp} = 525 F/g was attained at 10 mVs^{-1} in 0.1M H$_2$SO$_4$. Clearly, it can be seen from Table 3 that the specific capacitance and scan rate are inversely related. With an increase in scan rates, capacitance will be low owing to low charge storage ability of electrode material [64]. Enhanced specific capacitance with small area utilization by ions of electrolyte at a low scan rate is important to note down [65]. Synthesized $Ti_3C_2T_x/Ag_2CrO_4$ nanocomposite exhibits comparatively improved capacitance output even at lower concentration of acidic electrolyte. Comparison of $Ti_3C_2T_x/Ag_2CrO_4$ nanocomposite with other nanocomposites shown in Table 4.
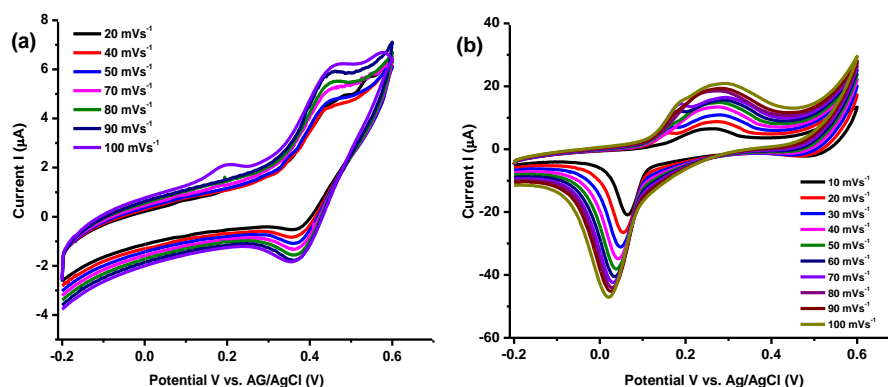

Figure 9. Voltametric profiles using $Ti_3C_2T_x/Ag_2CrO_4$ electrode (**a**) in 1 M KOH (**b**) 0.1 M H$_2$SO$_4$.

Table 4. Comparison of the specific capacitance with earlier MXene based nanocomposite electrodes.

Electrode	Electrolyte	Scan Rate (mVs^{-1})	Capacitance (F/g)	References
$Ti_3C_2T_x/Ag_2CrO_4$	0.1M H_2SO_4	10	525	This work
$Ti_3C_2T_x$ Aerogels	3M H_2SO_4	10	438	[66]
$Ti_3C_2T_x$ ion gel	Ionic liquid	20	70	[67]
Ti_3C_2Tx/PPy	1M H_2SO_4	5	416	[68]
Ti_3C_2Tx/PPy nanoparticles	1M Na_2SO_4	2	184.36	[69]

4. Conclusions

MXene ($Ti_3C_2T_x$) based silver-chromite nanocomposite special treatment particularly in the field of energy storage application is reported. XRD showed enhanced inter-planar spacing from 4.7 Å to 6.2 Å. SEM images revealed silver chromite nanoparticles attachment to MXene sheets whereas EDX confirmed the presence of silver chromite within the nanocomposite. Raman spectroscopy and photoluminescence revealed functional groups' attachment and a band gap value of about 3.86 eV. MXene/Ag_2CrO_4 nanocomposite-based electrode in 0.1M H_2SO_4 electrolyte have 525 F/g capacitance at a scan rate of 10 mVs^{-1} instead of its lower value of 75 F/g at 20 mVs^{-1} in case of 1M KOH. Thus, pseudocapacitive behavior in the acidic media gives maximum charge storage in the case of the $Ti_3C_2T_x/Ag_2CrO_4$ electrode, as compared to basic media. MXene type materials in nanocomposite form with significant capacitance in the near panorama give strategy to suggest more search. Here specific capacity of $Ti_3C_2T_x/Ag_2CrO_4$ electrode faraway from ideal value, for this reason there is need for progress in the instruction about surface functional groups.

Author Contributions: Conceptualization, T.Y. methodology, T.Y.; software, R.S.; validation, R.S., N.K.J. and M.R.; formal analysis, N.K.J.; investigation, S.K.; resources, A.A.A.-K. and A.A.; data curation, A.M. and S.K.; writing—original draft preparation, A.M.; writing—review and editing, A.A.S.; visualization, A.A.; supervision, A.A.S.; project administration, M.R.; funding acquisition, A.A.A.-K. All authors have read and agreed to the published version of the manuscript.

Institutional Review Board Statement: Not applicable.

Informed Consent Statement: Not applicable.

Data Availability Statement: All the data is contained in the manuscript.

Conflicts of Interest: The authors declare no conflict of interest.

References

1. Goel, A.; Kumar, M. Supercapacitors as energy storing device: A review. *Eur. J. Mol. Clin. Med.* **2020**, *7*, 3586–3594.
2. Saikia, B.K.; Benoy, S.M.; Bora, M.; Tamuly, J.; Pandey, M.; Bhattacharya, D. A brief review on supercapacitor energy storage devices and utilization of natural carbon resources as their electrode materials. *Fuel* **2020**, *282*, 118796. [CrossRef]
3. Lukatskaya, M.R.; Kota, S.; Lin, Z.; Zhao, M.-Q.; Shpigel, N.; Levi, M.D.; Halim, J.; Taberna, P.-L.; Barsoum, M.W.; Simon, P.; et al. Ultra-high-rate pseudocapacitive energy storage in two-dimensional transition metal carbides. *Nat. Energy* **2017**, *2*, 17105. [CrossRef]
4. Hu, H.; Pei, Z.; Ye, C. Recent advances in designing and fabrication of planar micro-supercapacitors for on-chip energy storage. *Energy Storage Mater.* **2015**, *1*, 82–102. [CrossRef]

5. Zhu, Q.; Li, J.; Simon, P.; Xu, B. Two-dimensional MXenes for electrochemical capacitor applications: Progress, challenges and perspectives. *Energy Storage Mater.* **2021**, *35*, 630–660. [CrossRef]

6. Chen, X.; Zhao, Y.; Li, L.; Wang, Y.; Wang, J.; Xiong, J.; Du, S.; Zhang, P.; Shi, X.; Yu, J. MXene/polymer nanocomposites: Preparation, properties, and applications. *Polym. Rev.* **2021**, *61*, 80–115. [CrossRef]

7. Jun, B.-M.; Kim, S.; Heo, J.; Park, C.M.; Her, N.; Jang, M.; Huang, Y.; Han, J.H.; Yoon, Y. Review of MXenes as new nanomaterials for energy storage/delivery and selected environmental applications. *Nano Res.* **2019**, *12*, 471–487. [CrossRef]

8. Osti, N.; Naguib, M.; Ostadhossein, A.; Xie, Y.; Kent, P.R.C.; Dyatkin, B.; Rother, G.; Heller, W.; Van Duin, A.C.T.; Gogotsi, Y.; et al. Effect of metal ion intercalation on the structure of MXene and water dynamics on its internal surfaces. *ACS Appl. Mater. Interfaces* **2016**, *8*, 8859–8863. [CrossRef]

9. Peng, Y.-Y.; Akuzum, B.; Kurra, N.; Zhao, M.-Q.; Alhabeb, M.; Anasori, B.; Kumbur, E.C.; Alshareef, H.N.; Ger, M.-D.; Gogotsi, Y. All-MXene (2D titanium carbide) solid-state microsupercapacitors for on-chip energy storage. *Energy Environ. Sci.* **2016**, *9*, 2847–2854. [CrossRef]

10. Iro, Z.S.; Subramani, C.; Dash, S.S. A brief review on electrode materials for supercapacitor. *Int. J. Electrochem. Sci.* **2016**, *11*, 10628–10643. [CrossRef]

11. Yang, J.; Bao, W.; Jaumaux, P.; Zhang, S.; Wang, C.; Wang, G. MXene-based composites: Synthesis and applications in rechargeable batteries and supercapacitors. *Adv. Mater. Interfaces* **2019**, *6*, 1802004. [CrossRef]

12. Shi, M.; Xin, Y.; Chen, X.; Zou, K.; Jing, W.; Sun, J.; Chen, Y.; Liu, Y. Coal-derived porous activated carbon with ultrahigh specific surface area and excellent electrochemical performance for supercapacitors. *J. Alloys Comp.* **2021**, *859*, 157856. [CrossRef]

13. Ghidiu, M.; Lukatskaya, M.R.; Zhao, M.-Q.; Gogotsi, Y.; Barsoum, M.W. Conductive two-dimensional titanium carbide 'clay' with high volumetric capacitance. *Nat. Cell Biol.* **2014**, *516*, 78–81. [CrossRef] [PubMed]

14. Yuan, C.; Bin Wu, H.; Xie, Y.; Lou, X.W. Mixed transition-metal oxides: Design, synthesis, and energy-related applications. *Angew. Chem. Int. Ed.* **2014**, *53*, 1488–1504. [CrossRef] [PubMed]

15. Xue, Y.; Sun, S.; Wang, Q.; Dong, Z.; Liu, Z. Transition metal oxide-based oxygen reduction reaction electrocatalysts for energy conversion systems with aqueous electrolytes. *J. Mater. Chem. A* **2018**, *6*, 10595–10626. [CrossRef]

16. Maitra, S.; Mitra, R.; Nath, T. Sol-gel derived $MgCr_2O_4$ nanoparticles for aqueous supercapacitor and alkaline OER and HER bi-functional electrocatalyst applications. *J. Alloys Comp.* **2021**, *858*, 157679. [CrossRef]

17. Veksha, A.; Moo, J.G.S.; Krikstolaityte, V.; Oh, W.-D.; Udayanga, W.C.; Giannis, A.; Lisak, G. Synthesis of $CaCr2O4$/carbon nanoplatelets from non-condensable pyrolysis gas of plastics for oxygen reduction reaction and charge storage. *J. Electroanal. Chem.* **2019**, *849*, 113368. [CrossRef]

18. Walia, S.; Balendhran, S.; Nili, H.; Zhuiykov, S.; Rosengarten, G.; Wang, Q.H.; Bhaskaran, M.; Sriram, S.; Strano, M.S.; Kalantar-Zadeh, K. Transition metal oxides—Thermoelectric properties. *Prog. Mater. Sci.* **2013**, *58*, 1443–1489. [CrossRef]

19. Ouyang, S.; Li, Z.; Ouyang, Z.; Yu, T.; Ye, J.; Zou, Z. Correlation of Crystal structures, electronic structures, and photocatalytic properties in a series of Ag-based oxides: $AgAlO_2$, $AgCrO_2$, and Ag_2CrO_4. *J. Phys. Chem. C* **2008**, *112*, 3134–3141. [CrossRef]

20. Xu, D.; Cheng, B.; Cao, S.; Yu, J. Enhanced photocatalytic activity and stability of Z-scheme Ag2CrO4-GO composite photocatalysts for organic pollutant degradation. *Appl. Catal. B Environ.* **2015**, *164*, 380–388. [CrossRef]

21. Feizpoor, S.; Habibi-Yangjeh, A.; Vadivel, S. Novel TiO_2/Ag_2 CrO_4 nanocomposites: Efficient visible-light-driven photocatalysts with n–n heterojunctions. *J. Photochem. Photobiol. A Chem.* **2017**, *341*, 57–68. [CrossRef]

22. Li, H.; Li, X.; Liang, J.; Chen, Y. Hydrous RuO_2-decorated MXene coordinating with silver nanowire inks enabling fully printed micro-supercapacitors with extraordinary volumetric performance. *Adv. Energy Mater.* **2019**, *9*, 1902467. [CrossRef]

23. Ma, Z.; Kang, S.; Ma, J.; Shao, L.; Zhang, Y.; Liu, C.; Wei, A.; Xiang, X.; Wei, L.; Gu, J. Ultraflexible and mechanically strong double-layered aramid nanofiber-Ti_3C_2Tx MXene/silver nanowire nanocomposite papers for high-performance electromagnetic interference shielding. *ACS Nano* **2020**, *14*, 8368–8382. [CrossRef]

24. Etman, A.S.; Halim, J.; Rosen, J. Fabrication of Mo1.33CTz (MXene)—Cellulose freestanding electrodes for supercapacitor applications. *Mater. Adv.* **2021**, *2*, 743–753. [CrossRef]

25. He, X.; Liu, Z.; Shen, G.; He, X.; Liang, J.; Zhong, Y.; Liang, T.; He, J.; Xin, Y.; Zhang, C.; et al. Microstructured capacitive sensor with broad detection range and long-term stability for human activity detection. *NPJ Flex. Electron.* **2021**, *5*, 17. [CrossRef]

26. Liu, Y.; Luo, R.; Li, Y.; Qi, J.; Wang, C.; Li, J.; Sun, X.; Wang, L. Sandwich-like Co_3O_4/MXene composite with enhanced catalytic performance for Bisphenol A degradation. *Chem. Eng. J.* **2018**, *347*, 731–740. [CrossRef]

27. Zou, G.; Zhang, Z.; Guo, J.; Liu, B.; Zhang, Q.; Fernandez, C.; Peng, Q. Synthesis of MXene/Ag composites for extraordinary long cycle lifetime lithium storage at high rates. *ACS Appl. Mater. Interfaces* **2016**, *8*, 22280–22286. [CrossRef] [PubMed]

28. Simon, P.; Gogotsi, Y. Materials for electrochemical capacitors. In *Nanoscience and Technology: A Collection of Reviews from Nature Journals*; Rodgers, P., Ed.; Macmillan: London, UK; World Scientific: London, UK, 2009; pp. 320–329.

29. Gao, Y.; Wang, L.; Zhou, A.; Li, Z.; Chen, J.; Bala, H.; Hu, Q.; Cao, X. Hydrothermal synthesis of TiO_2/Ti_3C_2 nanocomposites with enhanced photocatalytic activity. *Mater. Lett.* **2015**, *150*, 62–64. [CrossRef]

30. Iqbal, M.A.; Ali, S.I.; Amin, F.; Tariq, A.; Rizwan, S. La- and Mn-codoped bismuth ferrite/Ti3C2 MXene composites for efficient photocatalytic degradation of congo red dye. *ACS Omega* **2019**, *4*, 8661–8668. [CrossRef] [PubMed]

31. Shafique, R.; Rani, M.; Mahmood, A.; Khan, S.; Janjua, N.K.; Sattar, M.; Batool, K.; Yaqoob, T. Copper chromite/graphene oxide nanocomposite for capacitive energy storage and electrochemical applications. *Int. J. Environ. Sci. Technol.* **2021**. [CrossRef]

32. Alamdari, R.F.; Hajimirsadeghi, S.S.; Kohsari, I. Synthesis of silver chromate nanoparticles: Parameter optimization using Taguchi design. *Inorg. Mater.* **2010**, *46*, 60–64. [CrossRef]

33. Peng, C.; Yang, X.; Li, Y.; Yu, H.; Wang, H.; Peng, F. Hybrids of two-dimensional Ti_3C_2 and TiO_2 exposing {001} Facets toward enhanced photocatalytic activity. *ACS Appl. Mater. Interfaces* **2016**, *8*, 6051–6060. [CrossRef] [PubMed]

34. Zhou, L.; Kamyab, H.; Surendar, A.; Maseleno, A.; Ibatova, A.Z.; Chelliapan, S.; Karachi, N.; Parsaee, Z. Novel Z-scheme composite Ag2CrO4/NG/polyimide as high performance nano catalyst for photoreduction of CO_2: Design, fabrication, characterization and mechanism. *J. Photochem. Photobiol. A Chem.* **2019**, *368*, 30–40. [CrossRef]

35. Soofivand, F.; Mohandes, F.; Salavati-Niasari, M. Silver chromate and silver dichromate nanostructures: Sonochemical synthesis, characterization, and photocatalytic properties. *Mater. Res. Bull.* **2013**, *48*, 2084–2094. [CrossRef]

36. Tariq, A.; Ali, S.I.; Akinwande, D.; Rizwan, S. Efficient visible-light photocatalysis of 2D-MXene nanohybrids with Gd_3+- and Sn_4+-codoped bismuth ferrite. *ACS Omega* **2018**, *3*, 13828–13836. [CrossRef]

37. Irfan, S.; Rizwan, S.; Shen, Y.; Li, L.; Asfandiyar, A.; Butt, S.; Nan, C.-W. The gadolinium (Gd_3+) and tin (Sn_4+) co-doped $BiFeO_3$ nanoparticles as new solar light active photocatalyst. *Sci. Rep.* **2017**, *7*, 1–12. [CrossRef]

38. Vanaja, M.; Annadurai, G. Coleus aromaticus leaf extract mediated synthesis of silver nanoparticles and its bactericidal activity. *Appl. Nanosci.* **2013**, *3*, 217–223. [CrossRef]

39. Kannan, K.; Sliem, M.H.; Abdullah, A.M.; Sadasivuni, K.K.; Kumar, B. Fabrication of ZnO-Fe-MXene based nanocomposites for efficient CO_2 reduction. *Catalysts* **2020**, *10*, 549. [CrossRef]

40. Dong, X.; Li, J.; Xing, Q.; Zhou, Y.; Huang, H.; Dong, F. The activation of reactants and intermediates promotes the selective photocatalytic NO conversion on electron-localized Sr-intercalated g-C_3N_4. *Appl. Catal. B Environ.* **2018**, *232*, 69–76. [CrossRef]

41. Malik, T.; Naveed, S.; Muneer, M.; Mohammad, M.A. Fabrication and characterization of laser scribed supercapacitor based on polyimide for energy storage. *Key Eng. Mater.* **2018**, *778*, 181–186. [CrossRef]

42. Bin-In, J.; Hsia, B.; Yoo, J.-H.; Hyun, S.; Carraro, C.; Maboudian, R.; Grigoropoulos, C.P. Facile fabrication of flexible all solid-state micro-supercapacitor by direct laser writing of porous carbon in polyimide. *Carbon* **2015**, *83*, 144–151. [CrossRef]

43. Reddy, R.N.; Reddy, R.G. Sol-gel MnO_2 as an electrode material for electrochemical capacitors. *J. Power Sources* **2003**, *124*, 330–337. [CrossRef]

44. Naguib, M.; Mashtalir, O.; Carle, J.; Presser, V.; Lu, J.; Hultman, L.; Gogotsi, Y.; Barsoum, M.W. Two-dimensional transition metal carbides. *ACS Nano* **2012**, *6*, 1322–1331. [CrossRef] [PubMed]

45. Zhan, X.; Si, C.; Zhou, J.; Sun, Z. MXene and MXene-based composites: Synthesis, properties and environment-related applications. *Nanoscale Horiz.* **2019**, *5*, 235–258. [CrossRef]

46. Khan, T.M.; Mehmood, M.F.; Mahmood, A.; Shah, A.; Raza, Q.; Iqbal, A.; Aziz, U. Synthesis of thermally evaporated ZnSe thin film at room temperature. *Thin Solid Films* **2011**, *519*, 5971–5977. [CrossRef]

47. Nagarajan, R.D.; Sundaramurthy, A.; Sundramoorthy, A.K. Synthesis and characterization of MXene (Ti3C2Tx)/Iron oxide composite for ultrasensitive electrochemical detection of hydrogen peroxide. *Chemosphere* **2021**, *286*, 131478. [CrossRef]

48. Sarycheva, A.; Gogotsi, Y. Raman spectroscopy analysis of the structure and surface chemistry of Ti_3C_2Tx MXene. *Chem. Mater.* **2020**, *32*, 3480–3488. [CrossRef]

49. Hu, M.; Li, Z.; Hu, T.; Zhu, S.; Zhang, C.; Wang, X. High-capacitance mechanism for Ti_3C_2Tx MXene by in situ electrochemical raman spectroscopy investigation. *ACS Nano* **2016**, *10*, 11344–11350. [CrossRef] [PubMed]

50. Zhao, L.; Wang, K.; Wei, W.; Wang, L.; Han, W. High-performance flexible sensing devices based on polyaniline/MXene nanocomposites. *InfoMat* **2019**, *1*, 407–416. [CrossRef]

51. Muduli, S.; Pandey, P.; Devatha, G.; Babar, R.; Thripuranthaka, M.; Kothari, D.C.; Kabir, M.; Pillai, P.P.; Ogale, S.B. Photoluminescence quenching in self-assembled cspbbr3 quantum dots on few-layer black phosphorus sheets. *Angew. Chem.* **2018**, *130*, 7808–7812. [CrossRef]

52. Pan, A.; Ma, X.; Huang, S.; Wu, Y.; Jia, M.; Shi, Y.; Liu, Y.; Wangyang, P.; He, L.; Liu, Y. CsPbBr3 Perovskite nanocrystal grown on MXene nanosheets for enhanced photoelectric detection and photocatalytic CO_2 reduction. *J. Phys. Chem. Lett.* **2019**, *10*, 6590–6597. [CrossRef]

53. Iqbal, M.A.; Tariq, A.; Zaheer, A.; Gul, S.; Ali, S.I.; Akinwande, D.; Rizwan, S. Ti3C2-MXene/bismuth ferrite nanohybrids for efficient degradation of organic dyes and colorless pollutants. *ACS Omega* **2019**, *4*, 20530–20539. [CrossRef]

54. Ghifari, A.; Long, D.X.; Kim, S.; Ma, B.; Hong, J. Transparent platinum counter electrode prepared by polyol reduction for bifacial, dye-sensitized solar cells. *Nanomater.* **2020**, *10*, 502. [CrossRef]

55. Schechner, P.; Kroll, E.; Bubis, E.; Chervinsky, S.; Zussman, E. Silver-plated electrospun fibrous anode for glucose alkaline fuel cells. *J. Electrochem. Soc.* **2007**, *154*, B942–B948. [CrossRef]

56. Lufrano, F.; Staiti, P.; Minutoli, M. Influence of Nafion content in electrodes on performance of carbon supercapacitors. *J. Electrochem. Soc.* **2004**, *151*, A64–A68. [CrossRef]

57. Negroiu, R.; Svasta, P.; Pirvu, C.; Vasile, A.; Marghescu, C. Electrochemical impedance spectroscopy for different types of supercapacitors. In Proceedings of the 40th International Spring Seminar on Electronics Technology (ISSE), Sofia, Bulgaria, 10–14 May 2017.

58. Mujtaba, A.; Janjua, N.K. Fabrication and electrocatalytic application of CuO@Al_2O_3Hybrids. *J. Electrochem. Soc.* **2015**, *162*, H328–H337. [CrossRef]

59. Sabatani, E.; Rubinstein, I.; Maoz, R.; Sagiv, J. Organized self-assembling monolayers on electrodes. *J. Electroanal. Chem. Interfacial Electrochem.* **1987**, *219*, 365–371. [CrossRef]

60. Khan, S.; Shah, S.; Anjum, M.; Khan, M.; Janjua, N. Electro-oxidation of ammonia over copper oxide impregnated γ-Al_2O_3 nanocatalysts. *Coatings* **2021**, *11*, 313. [CrossRef]

61. Muhammad, S.; Zahra, U.B.; Ahmad, A.; Shah, L.A.; Muhammad, A. Understanding the basics of electron transfer and cyclic voltammetry of potassium ferricyanide—An outer sphere heterogeneous electrode reaction. *J. Chem. Soc. Pakistan* **2020**, *42*, 813–817.

62. Cossar, E.; Houache, M.S.; Zhang, Z.; Baranova, E.A. Comparison of electrochemical active surface area methods for various nickel nanostructures. *J. Electroanal. Chem.* **2020**, *870*, 114246. [CrossRef]

63. Xu, H.; Zheng, D.; Liu, F.; Li, W.; Lin, J. Synthesis of an MXene/polyaniline composite with excellent electrochemical properties. *J. Mater. Chem. A* **2020**, *8*, 5853–5858. [CrossRef]

64. Mishra, N.; Shinde, S.; Vishwakarma, R.; Kadam, S.; Sharon, M.; Sharon, M. MWCNTs synthesized from waste polypropylene plastics and its application in super-capacitors. In *AIP Conference Proceedings*; American Institute of Physics: College Park, MD, USA, 2013; Volume 1538, pp. 228–236. [CrossRef]

65. Sagadevan, S.; Chowdhury, Z.Z.; Bin Johan, M.R.; Aziz, F.A.; Salleh, E.M.; Hawa, A.; Rafique, R.F. A one-step facile route synthesis of copper oxide/reduced graphene oxide nanocomposite for supercapacitor applications. *J. Exp. Nanosci.* **2018**, *13*, 284–296. [CrossRef]

66. Wang, X.; Fu, Q.; Wen, J.; Ma, X.; Zhu, C.; Zhang, X.; Qi, D. 3D Ti_3C_2Tx aerogels with enhanced surface area for high performance supercapacitors. *Nanoscale* **2018**, *10*, 20828–20835. [CrossRef] [PubMed]

67. Lin, Z.; Barbara, D.; Taberna, P.-L.; Van Aken, K.L.; Anasori, B.; Gogotsi, Y.; Simon, P. Capacitance of Ti_3C_2Tx MXene in ionic liquid electrolyte. *J. Power Sources* **2016**, *326*, 575–579. [CrossRef]

68. Boota, M.; Anasori, B.; Voigt, C.; Zhao, M.-Q.; Barsoum, M.W.; Gogotsi, Y. Pseudocapacitive electrodes produced by oxidant-free polymerization of pyrrole between the layers of 2D titanium carbide (MXene). *Adv. Mater.* **2016**, *28*, 1517–1522. [CrossRef]

69. Zang, X.; Wang, J.; Qin, Y.; Wang, T.; He, C.; Shao, Q.; Zhu, H.; Cao, N. Enhancing capacitance performance of $Ti3C2Tx$ MXene as electrode materials of supercapacitor: From controlled preparation to composite structure construction. *Nano-Micro Lett.* **2020**, *12*, 77. [CrossRef]